Simultaneous Enhancement of Strength and Ductility in Cryogenically Treated AISI D2 Tool Steel

Hadi Ghasemi-Nanesa, Mohammad Jahazi[1],

Department of Mechanical Engineering, École de Technologie Supérieure, 1100 rue Notre-Dame Ouest, Montréal (QC) H3C 1K3 Canada.

Abstract:

In this research, the effect of cryogenic treatment on microstructural evolution and mechanical properties enhancement of AISI D2 tool steel was investigated. Cryogenic treatment down to liquid nitrogen temperature (77 K) was added to the conventional heat treatment between hardening and tempering steps. Electron microscopy investigation showed higher volume fraction of fine carbides with average diameter below 1µm indicating effective retardation in carbide coarsening process as a results of cryogenic treatment. A modification in types of carbides was also observed after cryogenic treatment. X-ray diffraction diagrams revealed transformation of retained austenite to martensite at cryogenic temperature. Weakening or removal of carbides peak in the X-ray diagram was considered as evidence of carbides different behavior at cryogenic temperature. Mechanical testing results indicated higher ultimate tensile strength, better ductility, and higher elastic modulus after cryogenic treatment. Analysis of stress-strain diagrams revealed different strain hardening behavior for cryogenically treated alloy when compared to the conventionally heat treated one. Fractography results confirmed strain hardening behavior and showed cleavage fracture for conventionally treated alloy but mixed cleavage - ductile fracture mode for cryogenically treated alloy. The improved mechanical properties after cryogenic treatment are interpreted in terms of the influence of higher volume fraction and uniform distribution of fine carbides in reducing the average active dislocations length and enhancement of the flow stress at any given plastic strain.

[1] Corresponding author: Prof. Mohammad Jahazi, E-mail: mohammad.jahazi@etsmtl.ca , Phone: 514 396-8974 Fax: 514 396-8530

Authors' accepted manuscript of the article published in Materials Science and Engineering: A, Vol. 598 http://dx.doi.org/10.1016/j.msea.2014.01.065

© 2014. Made available under the CC-BY-NC-ND 4.0 license http://creativecommons.org/licenses/by-nc-nd/4.0/

Keywords: A. Electron microscopy, A. Mechanical characterization, A. X-ray diffraction, B. Steel, D. Hardening, D. Precipitation.

1. Introduction

Tool steels are extensively used in modern industry for applications where high strength along with wear resistance and toughness are required [1]. These alloys are characterized by relatively large amounts of alloying elements such as tungsten, molybdenum, vanadium, and chromium and obtain their superior mechanical properties through heat treatment processes specific to each alloy [1-3]. The *conventional* heat treatment of tool steels consists of solutionizing in the austenitic region followed by quenching and simple or double tempering. The final microstructure of these steels is composed of martensite matrix, primary carbides, and secondary carbides (formed during the tempering step) and some undesired retained austenite [4, 5].

Cryogenic treatment is an additional process to the conventional heat treatment of tool steels originally intended to transform the residual austenite in the microstructure and therefore improve the wear resistance. The process involves cooling the materials down to liquid nitrogen temperature (77K), holding for specific time, and then heating up to room temperature (RT) followed by final tempering [4]. A number of cold work tool steels, high-speed tool steels, carburized steels, and stainless steels have been submitted to cryogenic treatments and the reports show considerable enhancement in wear resistance of these steels [6-10]. Despite the reported results on beneficial effects of cryogenic treatment, investigations about the fundamental mechanism governing cryogenic treatment and their effect on the microstructure of tool steels started only in late 1990's [6, 11-15].

Transformation of retained austenite to martensite, precipitation of fine η-carbides and relaxation of residual stresses reliefs have been suggested by researchers as possible mechanism responsible for the observed enhancement of wear resistance after cryogenic treatment [6]. However, these studies which mostly started in late 1990's are limited and have been carried out on different alloys and/or for different heat treatment conditions [6]. Moreover, in recent years in addition to superior wear resistance properties simultaneous high levels strength and ductility are also required, thereby further increasing the interest for a better understanding of the fundamental mechanisms governing the evolution of the microstructure during cryogenic treatment and its influence on the mechanical properties of tool steels [16-19].

AISI D2 tool steel is cold work tool steel with high strength and good wear resistance after conventional heat treatment but it suffers from poor ductility and brittle fracture. However, in most applications of AISI D2, high strength and good ductility are simultaneously required [7-10]. Although some authors have reported wear resistance enhancement of D2 steels after cryogenic treatment [7-10], others have reported hardness improvement but toughness reduction after cryogenic treatment [20]. More work is therefore required to better understand the interrelationships between cryogenic process parameters, microstructure evolution, and mechanical properties. The present work inscribes in this context and aims to study such interactions after cryogenic treatment of AISI D2 cutting tool steel with the view to find optimum combination of the tensile properties and ductility. In this regard, microstructure evolution and mechanical properties of conventionally and cryogenically treated specimens have been studied using advanced characterization methods and the obtained results analyzed in the framework of existing theories on dislocation interaction with carbon atoms and precipitates.

2. Experimental procedure

AISI D2 sheets with following chemical composition 1.54C, 0.33Si, 0.32Mn, 11.88Cr, 0.76Mo, 0.75V, 0.008P, and 0.008S (wt. %) were employed in this research. Samples were taken in random selection from a large industrial heat treatment batch. The heat treatment process was carried out in an industrial vacuum furnace, consisting of the following: 1) two preheating steps at 950 K and 1150 K, respectively; followed by temperature rise to 1300 K, 2) austenitization at 1300 K for 20 minutes followed by Argon quenching with a pressure of 2 bars at about 323K to avoid quench - cracking. For conventional heat treated alloy, three tempering cycles were conducted at 790K-2 hrs for each cycle. For cryogenic treatment, the plates were cooled down to 77K with a processing time of 4 hrs between quenching and tempering. After cryogenic treatment, two tempering cycles were applied at 790K and 780K, each with duration of 2 hrs. The schematics of heat treatment cycles for conventionally (a) and cryogenically (b) treated samples are shown in Fig.1.

For macrohardness measurement, Rockwell (C) hardness tester with major load of 150 kg was used. Sub-size samples for tensile tests were prepared according to ASTM-E8 standard. Uniaxial tensile tests were carried out using MTS793 machine with a crosshead speed of 1mm/min using extensometer in order to precisely measure mechanical properties including the ultimate tensile strength (UTS), the ultimate tensile strain, and the elastic modulus. To accurately examine the presence of phases, X-ray diffraction (XRD) analyses were conducted on as-quenched, conventionally treated, and cryogenically treated samples. Angular ranges of 35-105° 2θ with Cu-Kα radiation at 45kV and 40 mA and a step scanning at 0.02 $^\circ$ 2θ with count time of 1 second per point were used for the XRD experiments. 3% Nital solution was utilized for etching. Fractographical and microstructural investigations of both conventionally and

cryogenically treated samples were conducted using S3600N (Hitachi) conventional scanning electron microscope (SEM) and field emission SEM- SU70 (Hitachi). The volume fraction of carbides and other second phase particles were calculated using the MIP® image analysis software (Nahamin Pardazan Asia, www.metsofts.com).

3. Results

3.1. Microstructure characteristics

The initial microstructure before hardening treatment is usually the annealed condition (as-received alloy). In the annealed condition, the matrix is composed of ferrite and globular carbides as shown in Fig. 2. The larger carbides are mostly primary M_7C_3 carbides formed on the austenite grain boundaries and then dispersed as a result of hot working [21]. The other carbides such as M_2C and $M_{23}C_6$ are the result of secondary precipitation in the spherodiziation of carbides produced by the transformation of austenite on cooling after normalizing heat treatments. The formation of MC, M_2C (same chemical composition to M_7C_3 carbides), and $M_{23}C_6$ carbides are possible based on thermodynamic calculations [21].

Fig.3 shows SEM images from the microstructure of both conventionally and cryogenically treated specimens. The microstructure is composed of tempered martensite, primary carbides (PCs), large secondary carbides (LSCs), and small secondary carbides (SSCs). Comparison between microstructures obtained after cryogenic treatment and conventional treatment indicates that a higher volume fraction of SSCs is present in the microstructure after cryogenic treatment.

Further information about the size and volume fraction of secondary carbides was obtained from image analysis of the unetched microstructure. In fact, etching could cause higher volume fraction measurement due to the bigger perceptible area for carbides and lower amount for small

carbides (as they may be washed out during the etching process). Fig.4 shows the image analyses results about the size and volume fraction of carbides for (a) as-quenched condition, (b) conventionally treated, and (c) cryogenically treated samples.

In the present work, the carbides were divided in three ranges of sizes: (1) smaller than or equal to 1 µm (SSCs); (2) between 1 µm and 5 µm (LSCs); (3) larger than or equal to 5µm (PCs).Das et al. [14] have considered a forth range between 0.1 µm and 1 µm. However, Farina et al. [22] reported that image analysis around 0.1 µm does not show any differences between conventionally and cryogenically treated samples because of background noise effect. As shown in Fig.4b and c, after cryogenic treatment, the volume fraction of carbides with average diameter below 1 µm is higher than conventionally treated one and for carbides larger than or equal to 5 µm it is lower for the cryogenically treated sample. Hence, it can be assumed that cryogenic treatment in addition to delaying carbides coarsening, results in the formation of more fine carbides.

3.2. Crystallographic studies by XRD

XRD experiments were conducted on (a) as-quenched, (b) conventionally treated, and (c) cryogenically treated samples with the view to investigate the presence of various phases after each heat treatment, to study carbides behavior, and to measure carbon content of martensite using the (110) and (200) reflections with a method mentioned in Ref.23. Four peaks for martensite (M), one small peak for austenite-¥(222) just in as-quenched sample (Fig.5a), and carbides peaks for each heat treatment condition were identified by X'Pert HighScore software as well as by searching in the published literature [10,14] as illustrated in Fig.5. For 2θ angles between 35°- 55°, four peaks were detected corresponding to M_7C_3, Cr_7C_3, M_7C_3 and $M_{23}C_6$

carbides, and marteniste. The analysis of the results indicate that, M_7C_3 (420), Cr_7C_3 (150) carbides peaks show superposition close to 39° and M_7C_3 (202), Cr_7C_3 (112) peaks show superposition close to 42°. Small amounts of retained austenite, which were observed during the metallography examination process of the as-quenched condition has no trace in the XRD diagrams after both heat treatments.

For the conventionally heat treated sample, two superposed peaks of M_7C_3, Cr_7C_3 in 39° and 42° show intensity enhancement, which could be related to increase in the volume fraction of carbides. It should be mentioned that as the peak intensity of M_7C_3 (402) around 52.5° is almost identical for the three microstructural conditions therefore the observed augmentation in the peak intensity is related to Cr_7C_3 carbides. In contrast, for cryogenically treated specimens there is a reduction and even peak removal for Cr_7C_3 carbides in 39° and 42°. It is probable that the enhancement in the volume fraction of Cr_3C_7 carbides which takes place after conventional heat treatment has been significantly slowed down or even stopped by cryogenic treatment.

The carbon content of martensite shows the clear dependency of the matrix to the level of tetragonality in the crystal lattice. This factor was measured to be about 0.62 (wt. %) for the as-quenched sample, and 0.60 (wt. %) for the conventionally treated alloy. But this value was found to be 0.51 (wt. %) for cryogenically treated alloy indicating lower carbon content after cryogenic treatment. Lower carbon content was reported by Li et al. [24] on a cryogenically treated tool steel as well.

3.3. Mechanical properties

The influence of cryogenic treatment on mechanical properties was studied by conducting uniaxial tensile tests in both conventionally and cryogenically treated alloys as shown in Fig.6

(a-b). True stress (σ)-strain (ε) diagrams of cryogenically treated alloy showed 60 % ductility enhancement with 6% enhanced strength. Ductility enhancement after cryogenic treatment is analyzed in terms of its impact on the strain hardening coefficient θ (dσ/dε) and justified based on the theory proposed by Koneva and Kozlov [25].

The θ-ε diagram in Fig.6 a-b shows different stages in strain hardening behavior. The stage 1 shows strain independent positive and constant coefficient, θ, for both treated alloys. In stage 2, the parabolic behavior in which, θ decreases with more straining (ε) was observed. Stage 2 is finished with constant and nearly equal to zero value for θ. In stage3, θ is negative indicating that the neck develops. For the conventionally treated alloy, immediate fracture is observed in stage 3. By contrast, for cryogenically treated alloy, after stage 3, a fourth stage with negative and almost constant θ was observed. This post-uniform plastic strain, which is a major component of the total elongation and area-reduction, started after UTS.

SEM micrographs from the fracture surface of both conventionally and cryogenically treated samples are shown in Fig. 7 (a-c). The main characteristics of fracture surface are cleavage facets on PCs, cracking of PCs, and cracking at the interface between the PCs and the matrix (all shown in the area with dashed line) for both treated alloys. LSC and SSC particles are readily observable in fracture surfaces (shown by numbers 1 to 3). Unlike PCs, no cracking of SC particles could be identified on the fracture surfaces in both conventionally and cryogenically treated alloys. Generally, fracture starts with the cracking of primary carbides, cracking of primary carbides–matrix interfaces and nucleation of microvoids by decohesion of secondary carbides followed by cleavage fracture. However in the fracture surface of cryogenically treated sample, areas showing post uniform plastic deformation were observed (Fig.7c). The presence of

such features is indicative of partly ductile fracture of the material and confirms the occurrence of post-uniform plastic strain during tensile testing in cryogenically treated material.

Table1 shows the results for tensile tests of (a) conventionally treated, and (b) cryogenically treated samples and macrohardness measurements as well. Interestingly, simultaneous 60 % enhancement of ductility and 6 % enhanced UTS were observed after cryogenic treatment. Also, the slope of σ-ε curves for both treated alloys showed slight enhancement of the elastic modulus after cryogenic treatment which is in agreement with results reproduced by Baldissera et al. [17,18]. Li et al. [26] also have reported elastic modulus enhancement after cryogenic treatment with internal friction studies for a newly developed cold work die steel. The hardness measurement showed +1HRC enhancement for cryogenically treated sample which may be related to the transformation of retained austenite to martensite at cryogenic temperature. The Macrohardness enhancements in the range of +0.5 HRC to +4 HRD have been reported in the literature and related to retained austenite transformation to martensite during cryogenic treatment [6, 24].

4. Discussion

4.1. Variation in characteristics of small secondary carbides

Comparison of the XRD diagrams in Fig.5 (a to c) reveals that the higher intensity of the two superposed peaks observed around 39° and 42° in Fig.5b (i.e. after conventional heat treatment) can be associated with the rapid growth of Cr_3C_7 carbides. Das et al. [14] have reported that the presence of some Cr_7C_3 carbide along with alloyed carbides is inevitable in AISI D2 tool steel. Also Speich and Leslie [27] reported that in conventional tempering temperature range of 773K-873K, Cr addition delays the softening, but little or no secondary hardening take place because

Cr_7C_3 coarsens very rapidly at this tempering range. However, the XRD results for cryogenically treated specimens (Fig.5c) indicate that there is a reduction and even peak removal for Cr_3C_7 carbides around 39° and 42° after final tempering. As shown in Fig.4, the higher volume fraction of SSCs (<1micron diameter) after cryogenic treatment can be related to both retardation in the volume fraction enhancement of Cr_3C_7 carbides and dissolution of some Cr_3C_7 carbides (Fig.5c) as suggested by Tyshchenko et al. [28].

The proposed mechanism is based on the provision of more carbon atoms through the dissolution of primary carbides and the increased interactions of these carbon atoms with dislocations at cryogenic temperature. The interactions between carbon atoms, in saturated state, in the octahedral sites of martensite crystal lattice and dislocations form potential sites for SSCs nucleation at cryogenic temperature followed by precipitation during subsequent tempering [6, 28-31]. Also, studies on the effect of Cr on the dissolution of cementite in cold worked pearlitic steels indicated that Cr can increase the enthalpy of binding between carbon atoms and dislocations, but it doesn't show strong effect on the strengthening of interatomic bonds in the carbide's lattice [30-32]. On the basis of the above analysis, it can be reasonably assumed that the dissolution of some Cr_3C_7 carbides is occurring during cryogenic treatment which leads to XRD peak weakening or removal around 39° and 42° as well as higher volume fraction of SSCs (i.e. size <1μm diameter) after tempering.

4.2. On the enhancement of ductility

Fracture surface of conventionally treated sample indicates the brittle nature of the fracture (Fig.6a). Several origins have been reported for the observed brittle fracture including high tetragonality of martensite or high carbon content of martensite, fragmentation in large carbides

interfaces with matrix, temper embrittlement by segregation of embrittling elements such as Mn and Cr to prior austenite grain boundaries in the ~640K to ~840K temperature range, and austenite decomposition at tempering temperature leading to film-like cementite formation at the interface of austenite with martensite [27, 30, 32].

The results obtained in the present research indicate that a combination of the above factors has contributed to the observed brittleness of the alloy after conventional heat treatment. Specifically, the carbon content of martensite in the conventionally treated alloy is higher than that of the cryogenically treated one (0.61 wt% instead of 0.51 wt %). Although measurement of the level of martensite tetragonality before and after cryogenic treatment was out of the scope of the present work; however, such data has already been reported in the literature consistently [26, 33]. The enhanced intensity of Cr_3C_7 carbides peaks was observed (Fig.5b), the tempering temperature is in the range of temper embrittlement, and small amount of austenite has disappeared during conventional tempering (Fig.5b).

In contrast, for cryogenically treated sample, post-uniform plastic strain was observed (Fig.6b). The peak intensities of Cr_3C_7 carbides were weakened or removed after cryogenic treatment (Fig.5c). As the reduction in the peak intensity has direct relation with reduction in the volume fraction of each phase, it can therefore be said that the volume fraction of Cr_3C_7 has reduced after cryogenic treatment. The dissolution of some of Cr_3C_7 carbides in the microstructure aided to form nucleation sites for SSCs carbides (higher volume fraction of SSCs from Fig.4.c). It can be concluded that the ductility enhancement for tempered martensite after cryogenic treatment (Fig.7c and Table1) is related to a combined effect of lower carbon content of martensite and reduction in the volume fraction of Cr_3C_7 carbides (Fig.4c).

4.3. On the enhancement of strength

Fig.8 shows the stitched images taken from 3 different sections employed for the measurement of volume fraction of carbides with average diameter below 1μm for conventionally (a) and cryogenically (b) heat treated specimens, respectively. More uniform distribution of carbides was measured for cryogenically treated specimens. Precipitated carbides during tempering especially SSCs with average diameter ≤ 1μm (Fig.4c) provide strength enhancement (Table 1). Indeed dislocations cannot pass through incoherent precipitates such as SSCs, but they bow around and pass by the Orowan mechanism [34]. As the Orowan stress is inversely proportional to the distance between the precipitates, higher amounts of fine carbides with more uniform distribution reduces the average active dislocation link length and enhances the flow stress at any given plastic strain [32, 34].

The concomitant improvement of strength and ductility after cryogenic treatment can be related to three distinct microstructural changes: 1) higher volume fraction and more uniform distribution of carbides with average diameter below 1 μm (improvement of strength), 2) removing retained austenite by transformation to martensite (improvement of hardness) and 3) lower carbon content of martensite and reduction in the peak intensity of Cr_3C_7 carbides illustrated in XRD diagram of cryogenically treated alloy(improvement of ductility).

5. Conclusions

The influences of cryogenic treatment on microstructure evolution and mechanical properties of AISI D2 tool steel was studied and compared with conventional heat treatment. Simultaneous

enhancement of ductility and strength with higher elastic modulus was obtained for cryogenically treated alloy. Lower carbon content of martensite and higher volume fraction with more uniform distribution of carbides with average diameter below 1μm made major contributions to mechanical properties improvement in the cryogenically treated alloy. Also the transformation of retained austenite present after quenching to martensite at cryogenic temperature resulted in higher strength and hardness. The application of cryogenic treatment appears to have delayed the coarsening of precipitates; therefore no loss in tensile-strength properties was observed. Post-uniform plastic strain was observed for cryogenically treated alloy. The higher ductility level for cryogenically treated samples was further confirmed by fractography studies.

6. Acknowledgements

The authors would like to thank the National Sciences and Engineering Research Council of Canada (NSERC) for their support and financial contribution through the ENGAGE program. The authors also appreciate the collaboration of DK SPEC inc. in providing materials and experiments. Special thanks are due to Mr. Gil Trigo, Consultarc Inc. for valuable discussions throughout the project.

7. References

[1] A. P. Gulyaev Metallurgy. 12(1937) 65

[2] F. Meng, K. Tagashira, R. Azuma, H. Sohma, ISIJ Int. 34 (1994) 205-210.

[3] D. N. Collins, Heat Treat Met. 23(2) (1996) 40-42.

[4] ASM Handbook (1991) Vol. 4: Heat treating, ASM International, 1991.

[5] K. E. Thelning, Steels and its heat treatment, Butterworth & Co Publishers Ltd, London,1975.

[6] S. G. Singh, J. Singh, R. Singh, H. Singh, J Adv. Manuf. Technol. 54 (2011) 59-82.

[7] D. N. Collins, J. Dormer, Heat Treat Met. 24(3) (1997) 71-74.

[8] R. F. Barron, Cryogenics. 22 (1982) 409-413.

[9] D. Das, A.K. Dutta, K.K. Ray, Mater. Sci. Technol. 25 (2009) 1249-1257.

[10] D. Das, A.K. Dutta, K.K. Ray, Philos. Mag. Lett. 88 (2008) 801-811.

[11] D. Yun, L. Xiaoping, X. Honoshen, Heat Treat Met. 3(1998) 55-59.

[12] A. Bensely, A. Phadhakaran, L. Mohan, G. Nagarajan, Cryogenics. 45 (2005) 747-754.

[13] P. F. Stratton, Mater Sci Eng A.449-451 (2007) 809-812.

[14] D. Das, A. K. Dutta, K. K. Ray, Mater Sci Eng A.527 (9) (2010) 2182-2193.

[15] V. G. Gavriljuk, W. Theisen , V. V. Sirosh, E. V. Polshin, A. Kortmann, G. S. Mogilny, Y. N. Petrov, Y. V. Tarusin , Acta Mater.61(2013) 1705-1715.

[16] S. Zhirafar, A. Rezaeian, M. Pugh, J. Mater. Process. Technol. 186(1-3) (2007) 298-303.

[17] P. Baldissera, Mater. Des. 30 (2009) 3636-3642.

[18] P. Baldissera, C. Delprete, Mater. Des. 30 (2009) 1435-1440.

[19] S. Harish, A. Bensely, D. Mohan Lal, A. Rajadurai, Gyöngyvér B. Lenkey, J. Mater. Process. Tech. 209 (2009) 3351-3357.

[20] I. Wierszyllowski, Defect Diff. Forum. 258-260 (2006) 415-420.

[21] D. Bombac, M. Fazarinc, A. Saha Podder, G. Kugler, JMEPEG. 22(3) (2013) 742-747.

[22] P. F. da Silva Farina, C. A. Barbosa, H. Goldenstein, ASTM special technical publication.1532 (2012) 57-70.

[23] G. V. Kurdjumov, Metall. Trans. A 7 (1976) 999-1011.

[24] S. Li, Y. Xie, X. Wu, Cryogenics. 50 (2010) 89-92.

[25] N. A. Koneva, É. V. Kozlov, Soviet Physics Journal. 33(2) (1990) 2 165-179.

[26] S. Li, L. Deng, X. Wu, Cryogenics. 50(8) (2010) 433-438.

[27] G. R. Speich, W. C. Leslie, Metall. Trans. 3(5) (1972) 1043-1054.

[28] A.I. Tyshchenko, W. Theisen, A. Oppenkowski, S. Siebert, O.N. Razumov, A.P. Skoblik, V.A. Sirosh, Yu.N. Petrov, V.G. Gavriljuk, Mater Sci Eng A. 527 (2010) 7027-7039.

[29] L. Cheng, C.M. Brakman, B.M. Korevaar, E.J. Mittemeijer, Metall. Trans. A. 19 (1988) 2415-2426.

[30] K.A. Taylor, G.B. Olson, M. Cohen, J.B. Vander Sande, Metall. Trans. A. 20 (1989) 2749-2765.

[31] L. Cheng, N.M. van der Pers, A. Böttger, Th.H. de Keijser, E.J. Mittemeijer, Metall. Trans. A. 22 (1991) 1957-1967.

[32] G. Krauss, Mater. Sci. Eng. A. 273-275 (1999) 40-57.

[33] R. Kelkar, P. Nash, Y. Zhu, Heat Treat. Prog. ASM Int. 7 (2007) 57-60.

[34] D. Hull, D. J. Bacon, Introduction to Dislocations, Fifth ed., Butterworth- Heinemann, Burlington, 2011.

Figures Captions

Fig.1. Schematic representing typical time-temperature profile of the applied heat treatment cycles: (a) conventional heat treatment: austenitizing, quenching, and triple tempering (b) cryotreatment: austenitization, quenching, cryogenic cycle, and double tempering.

Fig.2. SEM micrograph of the starting microstructure of the AISI D2 tool steel (annealed condition). Matrix is composed of ferrite and globular carbides. Larger carbides are mostly primary M_7C_3 carbides. Small carbides are either M_2C or $M_{23}C_6$.

Fig.3. Effect of two applied heat treatment cycles on the presence of carbides with average diameter below 1 µm, in the microstructure of: (a) conventionally heat treated specimen and (b): cryotreated specimen. The microstructures revealed by etching with 3% Nital solution exhibit tempered martensite, primary carbide (PC), large secondary carbide (LSC), and small secondary carbide (SSC). Higher population of SCCs is clearly visible after (b).

Fig.4. Influence of cryotreatment process on the size distribution and volume fraction of carbides in comparison with conventional heat treatment using image analysis results from the microstructures of: (a) as-quenched, (b) conventionally heat treated, and (c) cryogenically treated samples. Higher volume fraction of carbides with average diameter below 1 µm was obtained after (c) in comparison with (b).

Fig.5. X-ray diffraction line profiles of (a) quenched, (b) conventionally heat treated, and (c) cryogenically treated specimens showing different evolution in carbides types after each treatment. Each profile represents the set of (hkl) indicating different diffraction planes of martensite, M_7C_3, $M_{23}C_6$, Cr_7C_3 carbides (existence of small (222) peak of retained austenite in the quenched sample). Retained austenite peak was eliminated after (b) and (c) treatments in different ways. Enhancement in the volume fraction of Cr_3C_7 carbides observed after conventional heat treatment (b) was slowed down or even stopped by (c) cryogenic treatment.

Fig.6. Simultaneous enhancement in strength and ductility from (a) conventionally heat treated sample to (b) cryogenically treated samples using true stress-strain(σ-ε) diagrams and related strain hardening behavior (θ-ε diagrams). θ is defined in the figure. In the case of the cryogenically treated samples (b) a fourth stage was revealed in the θ-ε diagram showing negative and almost constant θ (i.e. post-uniform plastic strain) indicating that cryogenic treatment results in concomitant increase of strength and ductility.

Fig.7. SEM micrographs from the fracture surface of (a) conventionally heat treated and (b) cryogenically treated samples after uniaxial tensile tests. Cleavage facets in primary carbides, cracking of primary carbides, indicated by red dashed lines, and dimples on secondary carbides, numbered from 1 to 3, are present for the two conditions. In (c) an area from sample (b) showing ductile fracture is illustrated.

Fig.8. The carbides with average diameters below 1 μm are highlighted by red spots in the image using image analyzing software to compare their volume fraction and distribution in (a) conventionally treated sample and (b) cryogenically treated one. Higher volume fractions with more uniform distribution of carbides is shown in (b) which results in higher UTS as indicated in mechanical testing results (Fig. 6).

Table Caption

Table1. Tensile test results for (a) conventionally heat treated and (b) cryogenically treated samples.

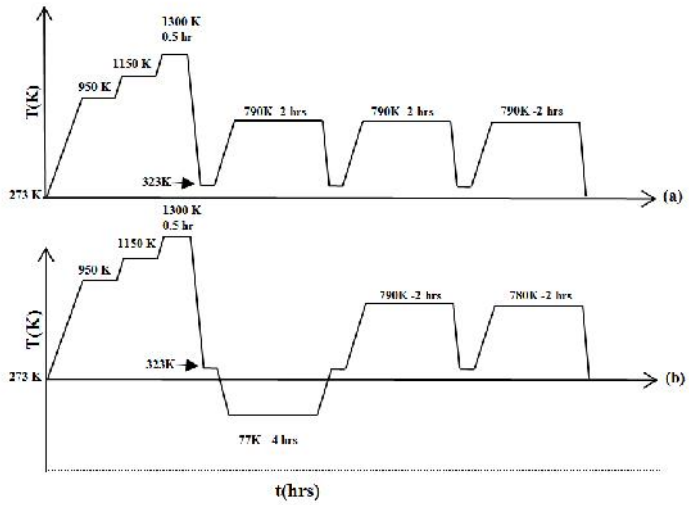

Fig.1. Schematic representing typical time-temperature profile of the applied heat treatment cycles: (a) conventional heat treatment: austenitizing, quenching, and triple tempering (b) cryotreatment: austenitization, quenching, cryogenic cycle, and double tempering.

.

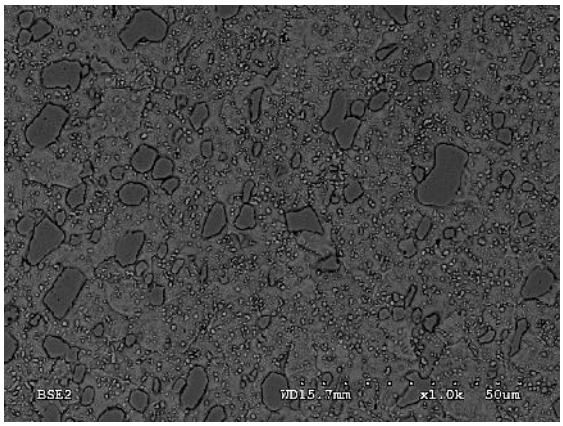

Fig.2. SEM micrograph of the starting microstructure of the AISI D2 tool steel (annealed condition). Matrix is composed of ferrite and globular carbides. Larger carbides are mostly primary M_7C_3 carbides. Small carbides are either M_2C or $M_{23}C_6$.

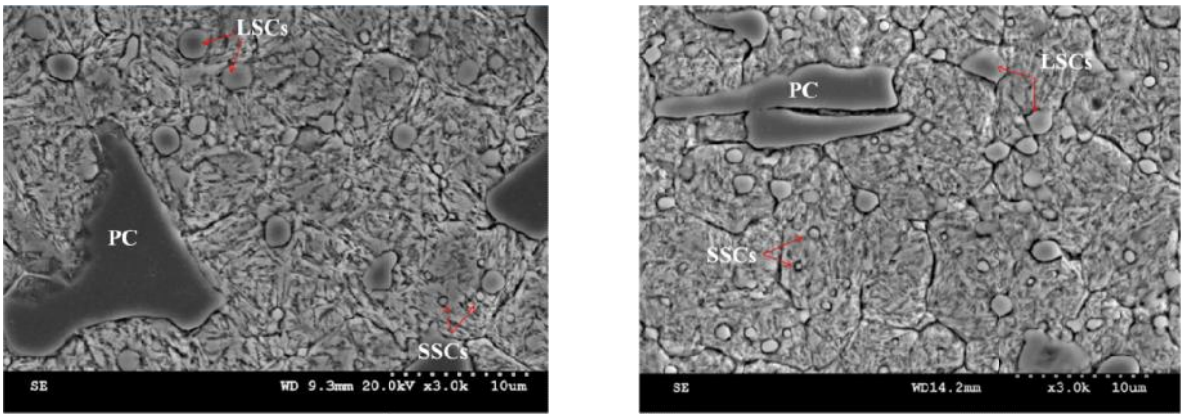

(a) (b)

Fig.3. Effect of two applied heat treatment cycles on the presence of carbides with average diameter below 1 µm, in the microstructure of: (a) conventionally heat treated specimen and (b): cryotreated specimen. The microstructures revealed by etching with 3% Nital solution exhibit tempered martensite, primary carbide (PC), large secondary carbide (LSC), and small secondary carbide (SSC). Higher population of SCCs is clearly visible after (b).

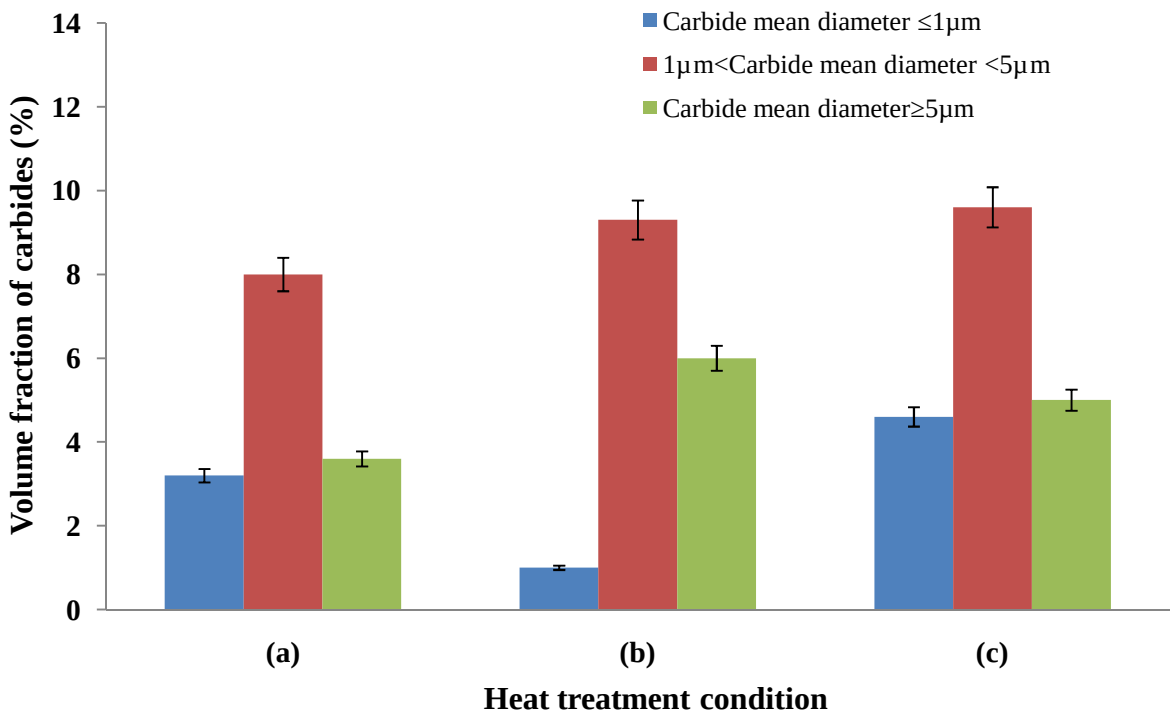

Fig.4. Influence of cryotreatment process on the size distribution and volume fraction of carbides in comparison with conventional heat treatment using image analysis results from the microstructures of: (a) as-quenched, (b) conventionally heat treated, and (c) cryogenically treated samples. Higher volume fraction of carbides with average diameter below 1 µm was obtained after (c) in comparison with (b).

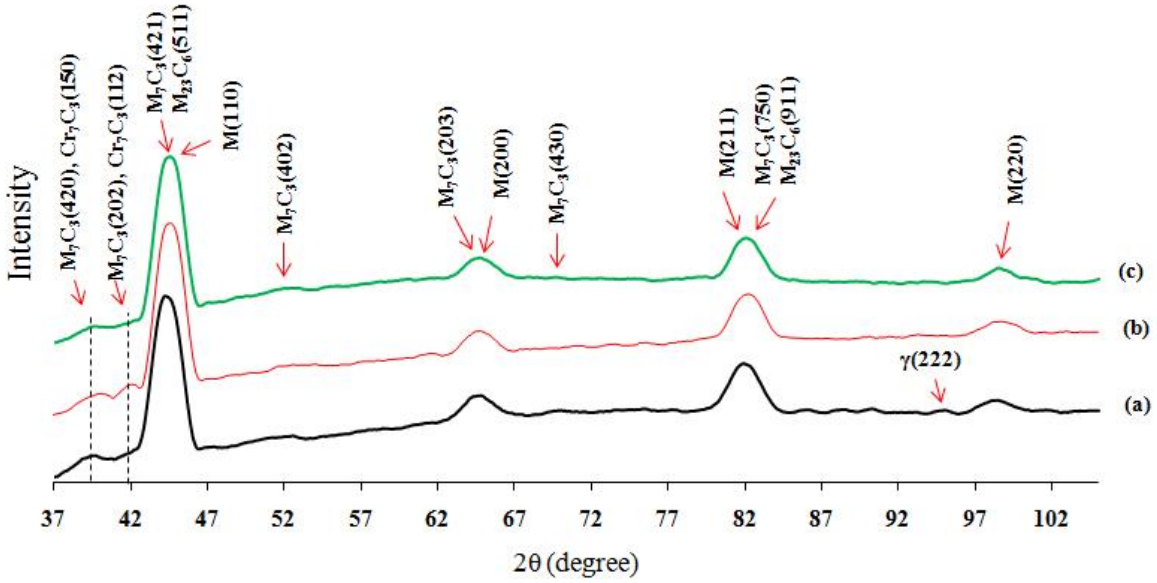

Fig.5. X-ray diffraction line profiles of (a) quenched, (b) conventionally heat treated, and (c) cryogenically treated specimens showing different evolution in carbides types after each treatment. Each profile represents the set of (hkl) indicating different diffraction planes of martensite, M_7C_3, $M_{23}C_6$, Cr_7C_3 carbides (existence of small (222) peak of retained austenite in the quenched sample). Retained austenite peak was eliminated after (b) and (c) treatments in different ways. Enhancement in the volume fraction of Cr_3C_7 carbides observed after conventional heat treatment (b) was slowed down or even stopped by (c) cryogenic treatment.

.

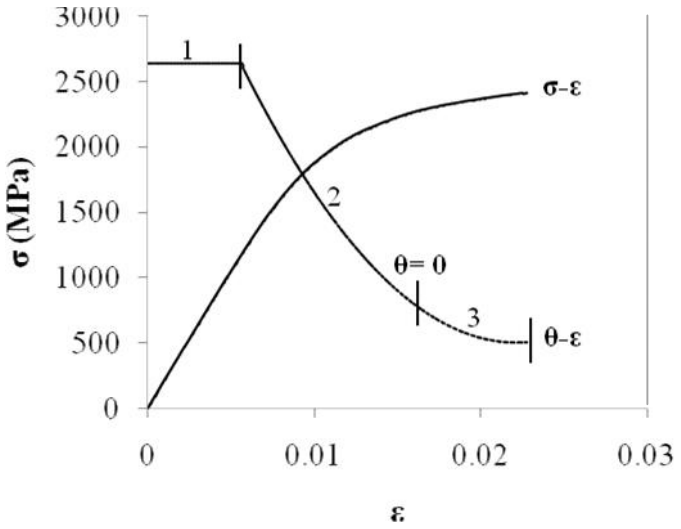

(a)

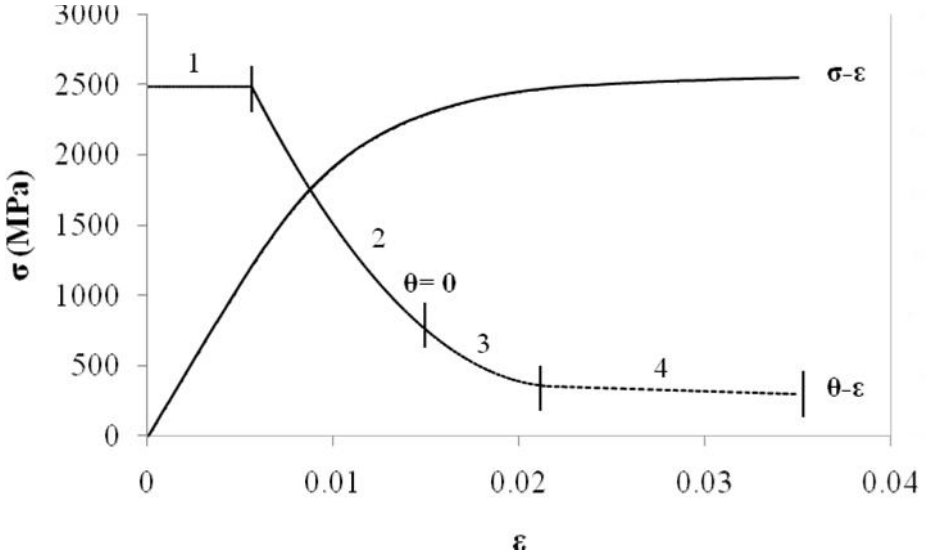

(b)

Fig.6. Simultaneous enhancement in strength and ductility from (a) conventionally heat treated sample to (b) cryogenically treated samples using true stress-strain(σ-ε) diagrams and related strain hardening behavior (θ-ε diagrams). θ is defined in the figure. In the case of the cryogenically treated samples (b) a fourth stage was revealed in the θ-ε diagram showing negative and almost constant θ (i.e. post-uniform plastic strain) indicating that cryogenic treatment results in concomitant increase of strength and ductility.

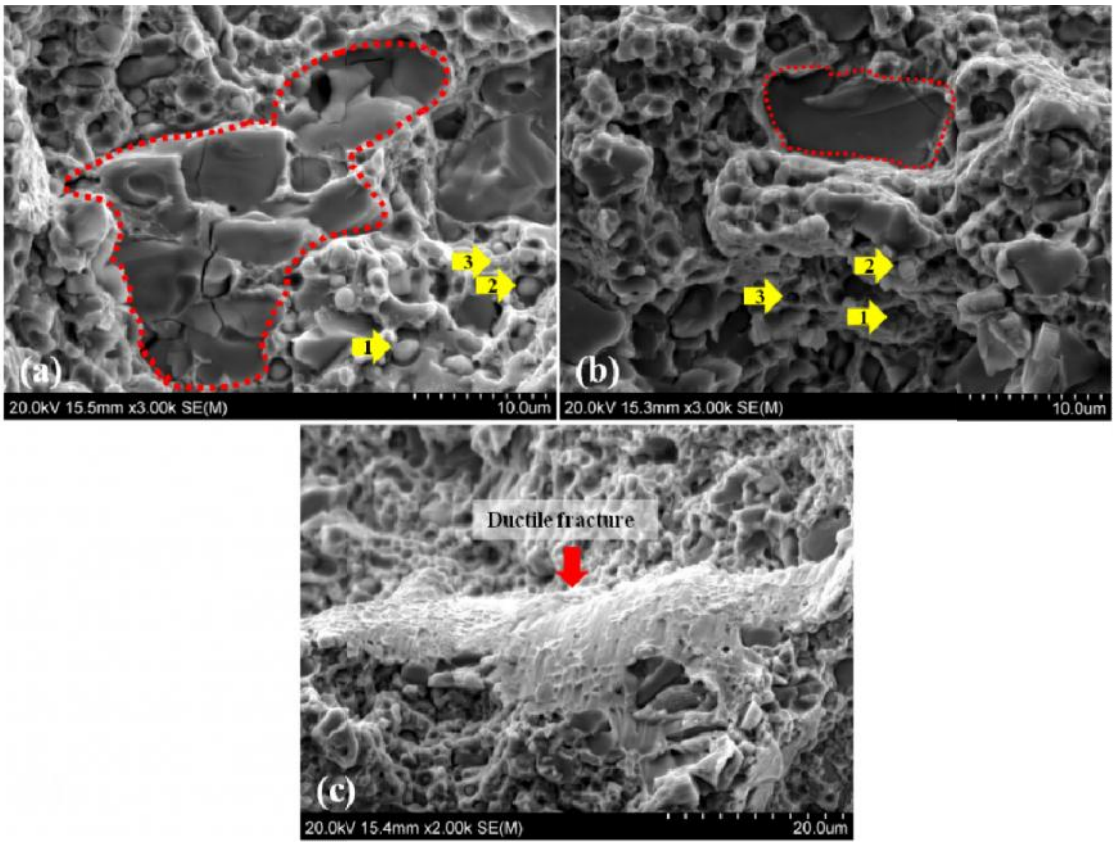

Fig.7. SEM micrographs from the fracture surface of (a) conventionally heat treated and (b) cryogenically treated samples after uniaxial tensile tests. Cleavage facets in primary carbides, cracking of primary carbides, indicated by red dashed lines, and dimples on secondary carbides, numbered from 1 to 3, are present for the two conditions. In (c) an area from sample (b) showing ductile fracture is illustrated.

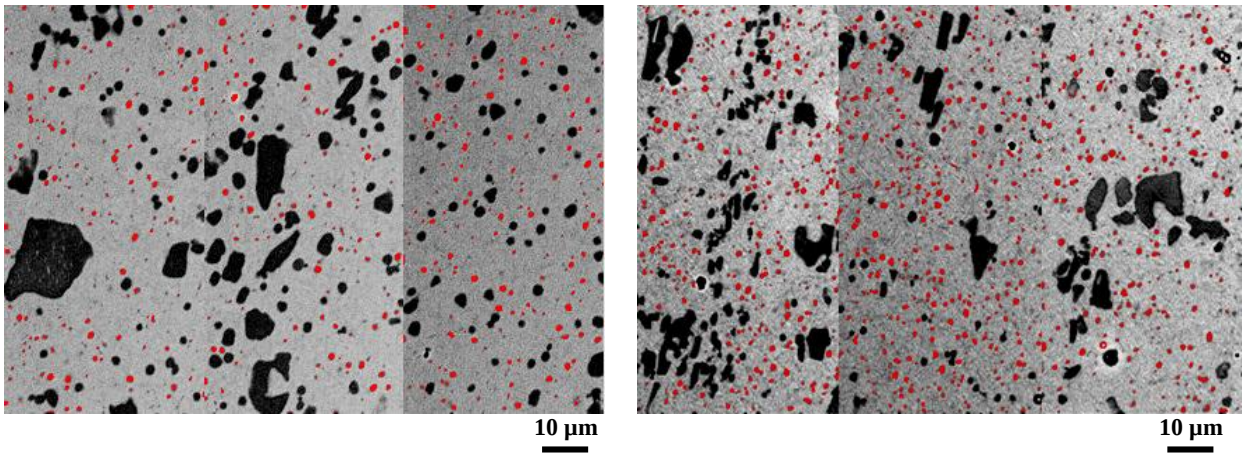

(a) (b)

Fig.8. The carbides with average diameters below 1 µm are highlighted by red spots in the image using image analyzing software to compare their volume fraction and distribution in (a) conventionally treated sample and (b) cryogenically treated one. Higher volume fractions with more uniform distribution of carbides is shown in (b) which results in higher UTS as indicated in mechanical testing results (Fig. 6).

Table1. Tensile test results for (a) conventionally heat treated, (b) cryogenically treated samples.

	UTS (MPa)	Ultimate tensile strain (ε)	Elastic Modulus (GPa)	Hardness (R_C)
a	2410	0.022	209	57
b	2550	0.035	214	58